Reaction of aluminum clusters with water

Satoshi Ohmura,[1,2] Fuyuki Shimojo,[1,2,a)] Rajiv K. Kalia,[1] Manaschai Kunaseth,[1] Aiichiro Nakano,[1,b)] and Priya Vashishta[1]
[1]*Collaboratory for Advanced Computing and Simulations, Department of Physics & Astronomy, Department of Chemical Engineering & Materials Science, and Department of Computer Science, University of Southern California, Los Angeles, California 90089-0242, USA*
[2]*Department of Physics, Kumamoto University, Kumamoto 860-8555, Japan*

(Received 16 February 2011; accepted 2 June 2011; published online 22 June 2011)

The atomistic mechanism of rapid hydrogen production from water by an aluminum cluster is investigated by *ab initio* molecular dynamics simulations on a parallel computer. A low activation-barrier mechanism of hydrogen production is found, in which a pair of Lewis acid and base sites on the cluster surface plays a crucial role. Hydrogen production is assisted by rapid proton transport in water via a chain of hydrogen-bond switching events similar to the Grotthuss mechanism, where hydroxide ions are converted to water molecules at the Lewis-acid sites and hydrogen atoms are supplied at the Lewis-base sites. The activation free energy is estimated along various reaction paths associated with hydrogen production, and the corresponding reaction rates are discussed based on the transition state theory. © *2011 American Institute of Physics*. [doi:10.1063/1.3602326]

I. INTRODUCTION

Exothermic reaction of metal particles with water produces hydrogen,[1–5] and the understanding of its atomistic mechanism has gained importance in the context of renewable energy.[6,7] Meanwhile, it has been realized that the chemical reactivity at the nanoscale differs drastically from its macroscopic counterpart.[8–10] For example, flame propagation speeds for metallic nanoparticles embedded in oxidizers are accelerated to km/s, compared with cm/s in the case of micron-size particles.[11] Such rapid nano-reaction cannot be explained by conventional mechanisms based on mass diffusion of reactants, and thus various mechanisms for enhanced nano-energetic reactions have been proposed.[11–13] For the case of aluminum (Al) clusters in oxidizers, these nano-reaction mechanisms include accelerated mass transport due to large residual stresses.[11–13] Furthermore, metal nanoclusters possess catalytic behaviors that are distinct from larger particles.[14–16] A remarkable example is size-selective reactivity of Al clusters with water,[17,18] where an anion of the Al cluster, Al_n^- (for instance, $n = 12$ or 17), reacts strongly with water molecules in gas phase. The enhanced reactivity has been attributed to the dissociative chemisorption of water at two specific surface sites that, respectively, act as a Lewis acid and a Lewis base where OH and H preferentially bind.[17,18] In the proposed gas-phase reaction mechanism with the adsorption of multiple water molecules onto an Al_{17} cluster, the energy barrier of the production of H_2 from two H atoms generated on the cluster surface has been estimated to be about 1 eV.[17] How the reactivity of these Al "superatoms"[17,19] changes in bulk water is of great interest both scientifically and technologically.

Here, we perform *ab initio* molecular dynamics simulations on a parallel computer to study the reaction of an Al_{17} cluster in bulk water, with the goal of exploring different mechanisms with more enhanced reactivity than the gas-phase mechanism mentioned above. We find rapid hydrogen-production processes, which are assisted by rapid proton transport[20,21] via a chain of hydrogen-bond switching events similar to the Grotthuss mechanism.[22–24] Although one of the hydrogen-production reactions observed in our molecular dynamics (MD) simulations has been reported earlier,[25] this paper is the first to provide a full description of all the reaction processes.

II. METHOD OF CALCULATION

The electronic states are calculated using the projector-augmented-wave (PAW) method,[26,27] which is an all-electron electronic-structure-calculation method within the frozen-core approximation. In the framework of density functional theory, the generalized gradient approximation[28] is used for the exchange-correlation energy with non-linear core corrections.[29] The momentum-space formalism is utilized,[30] where the plane-wave cutoff energies are 30 and 250 Ry for the electronic pseudo-wave functions and the pseudo-charge density, respectively. The energy functional is minimized iteratively using a preconditioned conjugate-gradient method.[31,32] The Γ point is used for Brillouin zone sampling. Projector functions are generated for the 3s, 3p, and 3d states of Al, the 2s and 2p states of O, and the 1s state of H.

The electronic-structure-calculation code has been implemented on parallel computers[32] by a hybrid approach combining spatial decomposition (i.e., distributing real-space or reciprocal-space grid points among processors) and band decomposition (i.e., assigning the calculations of different Kohn-Sham orbitals to different processors). The program has been implemented using the message passing interface library for interprocessor communications. The 6 ps simulations

a)Electronic mail: shimojo@kumamoto-u.ac.jp.
b)Electronic mail: anakano@usc.edu.

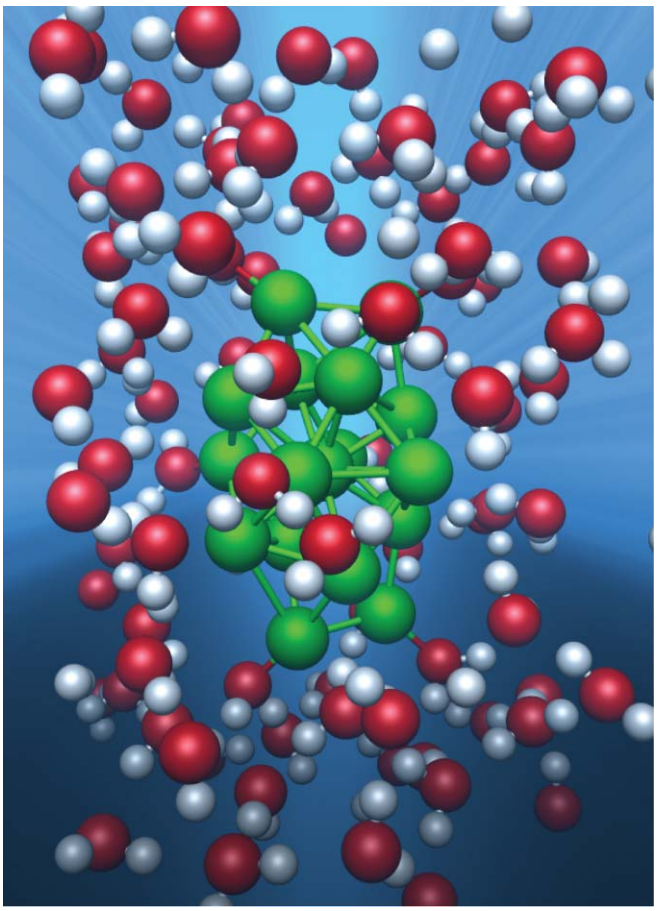

FIG. 1. Snapshot of the Al_{17} + water system, where green, red, and white spheres represent aluminum, oxygen, and hydrogen atoms, respectively.

reported here took 400 h on 64 AMD Opteron (2.33 GHz) processors.

MD simulations are carried out at temperatures of 300, 500, and 1000 K in the canonical ensemble using the Nosè-Hoover thermostat technique.[33,34] The equations of motion are integrated numerically using an explicit reversible integrator[35] with a time step of 11 a.u. (~0.264 fs). The system studied in our MD simulations consists of an Al_{17} cluster and 84 H_2O molecules (in total of 269 atoms) in a box of dimensions 12.58 ×12.58 × 18.87 Å^3 (see Fig. 1). The system size is determined from the density of water in the ambient condition, and periodic boundary conditions are imposed.

To quantify the change in the bonding properties of atoms associated with the hydrogen-production reaction, we use a bond-overlap population analysis[36,37] by expanding the electronic wave functions in an atomic-orbital basis set.[38,39] Based on the formulation generalized to the PAW method,[40] we obtain the gross population $Z_i(t)$ for the ith atom and the bond-overlap population $O_{ij}(t)$ for a pair of ith and jth atoms as a function of time t. From $Z_i(t)$, we estimate the charge of atoms, and $O_{ij}(t)$ gives a semi-quantitative estimate of the strength of covalent bonding between atoms. As the atomic-basis orbitals, we use numerical pseudo-atomic orbitals, which are obtained for a chosen atomic energy so that the first node occurs at the desired cutoff radius.[41] To increase

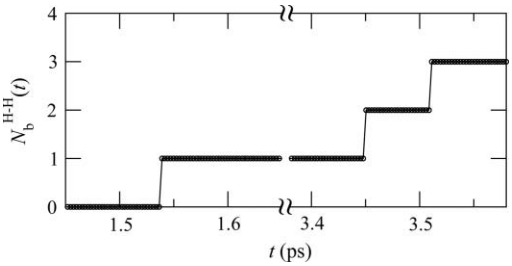

FIG. 2. Time evolution of the number of chemical bonds $N_b^{H-H}(t)$ for H–H. Two atoms are considered bonded when their distance is less than a cutoff distance $R_c = 1.0$ Å during a prescribed bond lifetime of 24 fs. (See Ref. 20.)

the efficiency of the expansion, the numerical basis orbitals are augmented with the split-valence method.[42] The resulting charge spillage, which estimates the error in the expansion, is only 0.3%, indicating the high quality of the basis orbitals.

III. RESULTS AND DISCUSSION

A. Hydrogen-production processes

In our simulation at room temperature (300 K), six water molecules bond to the Al cluster. Formation of these Al–O bonds enhances the Lewis-base character of Al atoms that are not connected to the water molecules, thereby preventing further bonding of water molecules to the Al clusters. Dissociation of water molecules is not observed within the limited simulation time (several ps) at this temperature. Even when the temperature is raised to 500 K, still no water molecule dissociates. The atomistic process of hydrogen production is successfully observed in MD simulation at 1000 K. Figure 2 shows the time evolution of the number of chemical bonds between two H atoms. In total, three hydrogen molecules are produced at 1.54, 3.45, and 3.51 ps, within the simulation time of 6 ps. As a reference, we have simulated water without an Al cluster at the same temperature. This simulation did not produce any hydrogen molecule, and it is therefore concluded that the Al cluster is necessary for the hydrogen production even at such a high temperature. Below, we describe the reaction processes observed in the MD simulation at 1000 K in detail in order to discuss reaction paths for hydrogen production. Here, we use the high-temperature simulation as a way to find transition paths in a very complex system within the timescale accessible to MD simulation. We will then discuss the kinetics of the reactions related to hydrogen production at room temperature based on the energy barriers along the found reaction paths, as will be discussed in Sec. III B.

To find the production mechanism of the three hydrogen molecules, we investigate the time evolution of atomic configuration along with bond-overlap populations $O_{ij}(t)$. Figure 3 shows the production process of the first hydrogen molecule observed at 1.54 ps. In the snapshot at 1.48 ps (Fig. 4), one H atom labeled "H1" bonds to an Al atom labeled "Al1," and one water molecule consisting of H2, H3, and O1 bonds to another Al atom labeled "Al3." In Fig. 3, $O_{ij}(t)$ for H1–Al1 and O1–Al3, as well as those for O1–H2 and O1–H3 within the water molecule, take finite values for $t < 1.5$ ps, signifying chemical bonds between these atoms. At about

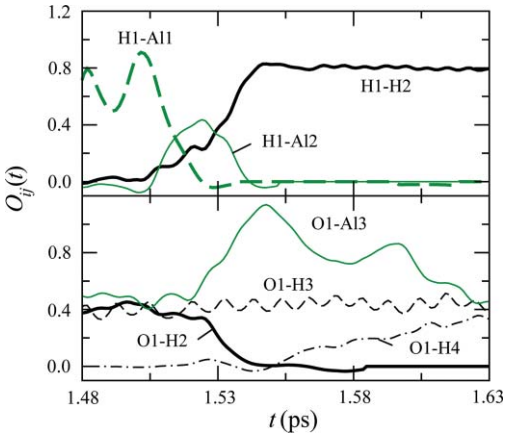

FIG. 3. Production process of the first hydrogen molecule on the Al cluster observed in MD simulation. Time evolution of bond-overlap populations $O_{ij}(t)$ associated with atoms labeled in the snapshots of atomic configurations in Fig. 4.

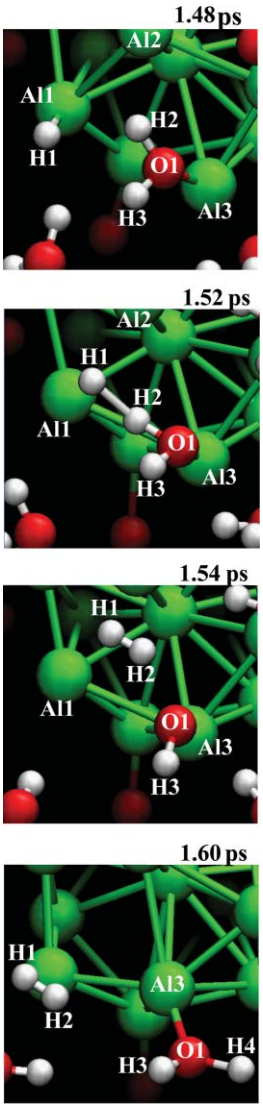

FIG. 4. Production process of the first hydrogen molecule on the Al cluster observed in MD simulation. Atomic configurations are shown at time t = 1.48, 1.52, 1.54, and 1.60 ps, where white, red, and green spheres represent H, O, and Al atoms, respectively.

1.5 ps, $O_{\mathrm{H1-H2}}(t)$ and $O_{\mathrm{H1-Al2}}(t)$ begin to increase (Al2 is an Al atom adjacent to Al3), and at the same time $O_{\mathrm{H1-Al1}}(t)$ decreases rapidly. In the snapshot at 1.52 ps in Fig. 4, H1 atom bonds partially to those three (H2, Al1, and Al2) atoms. While $O_{\mathrm{H1-Al2}}(t)$ decreases after 1.52 ps, $O_{\mathrm{H1-H2}}(t)$ continues to increase and maintains a quite large value ~0.8 after 1.54 ps, i.e., a hydrogen molecule (H1–H2) is formed as shown in the snapshots at 1.54 and 1.6 ps in Fig. 4. The chemical bond between O1 and Al3 strengthens as $O_{\mathrm{O1-Al3}}(t)$ exceeds 0.8, which is accompanied by the breakage of one of the O–H bonds (O1–H2) in the water molecule, leaving a hydroxide ion (O1–H3) at 1.54 ps. Subsequently, the OH group turns into a H_2O molecule by the Grotthuss mechanism[22–24] with another hydrogen atom (H4) supplied by surrounding water molecules (see the snapshot at 1.6 ps in Fig. 4). $O_{\mathrm{O1-H4}}(t)$ increases gradually after 1.55 ps, and simultaneously $O_{\mathrm{O1-Al3}}(t)$ decreases. This hydrogen-production reaction is summarized as

$$\mathrm{Al{-}OH_2 + Al{-}H \rightarrow Al{-}OH + Al + H_2}. \qquad (1)$$

As mentioned above, it is notable that the Al–OH product of this reaction thermally fluctuates back to Al–OH_2, the mechanism of which will be elucidated below.

The production mechanism of the second hydrogen molecule observed at 3.45 ps is almost the same as that of the first molecule. Figures 5 and 6 respectively, show the time evolution of $O_{ij}(t)$ and the atomic configuration in the production process of the second molecule. In the atomic configuration at 3.40 ps (Fig. 6), a H atom H5 is attached to an Al atom Al4, and a water molecule, consisting of O2, H6, and H7, is attached to another Al atom Al5. The chemical bonds for H5–Al4 and O2–Al5, as well as those for O2–H6 and O2–H7 within the water molecule, are reflected in the finite values of $O_{ij}(t)$ between these atoms for $t < 3.43$ ps, as shown in Fig. 5. At about 3.43 ps, $O_{\mathrm{H5-H6}}(t)$ starts to increase and maintains a fairly large value ~0.8 after 3.48 ps, i.e., the second hydrogen molecule (H5–H6) is formed as shown in the snapshots at 3.45 and 3.51 ps. Accompanying the formation of chemical bonds for H5–H6, those for H5–Al4 and O2–H6 are broken, as $O_{\mathrm{H5-Al4}}(t)$ and $O_{\mathrm{O2-H6}}(t)$ decreases to almost zero. A hydroxide ion (O2–H7), attached to Al5, is left, and this hydrogen-production reaction is again summarized as Eq. (1). Unlike the previous process, however, a third Al atom, such as Al2 in Figs. 3 and 4, is not involved in the process shown in Figs. 5 and 6, indicating that such Al atom is not necessary for the hydrogen production.

The third hydrogen molecule is produced at 3.51 ps in a different way from the former two cases (see Fig. 7). First, H atoms associated with four water molecules move by the Grotthuss mechanism as indicated by the yellow arrows in the snapshot at 3.5 ps. After the formation and breakage of some chemical bonds, the third hydrogen molecule, as well as a H_3O_2 product and two water molecules, are formed as displayed in the snapshot at 3.51 ps. After some OH-bond exchanges following the magenta arrows, the H_3O_2 product is dissolved into water molecules, leaving a hydroxide ion on the surface of the Al cluster (see the snapshot at

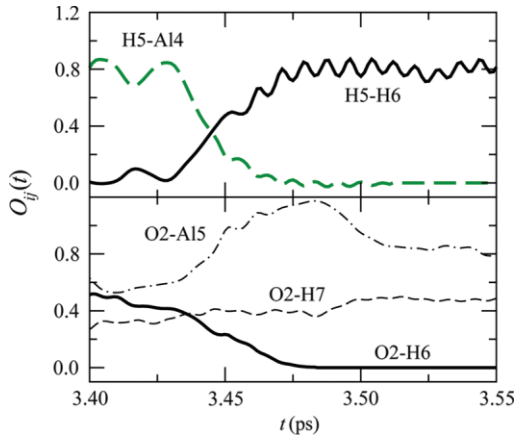

FIG. 5. Production process of the second hydrogen molecule on the Al cluster observed in MD simulation. Time evolution of bond-overlap populations $O_{ij}(t)$ associated with atoms labeled in the snapshots of atomic configurations in Fig. 6.

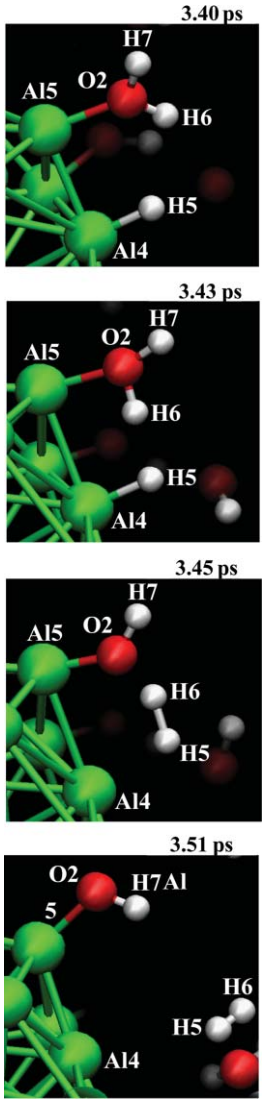

FIG. 6. Production process of the second hydrogen molecule on the Al cluster observed in MD simulation. Atomic configurations are shown at time $t = 3.40$, 3.43, 3.45, and 3.51 ps, where white, red, and green spheres represent H, O, and Al atoms, respectively.

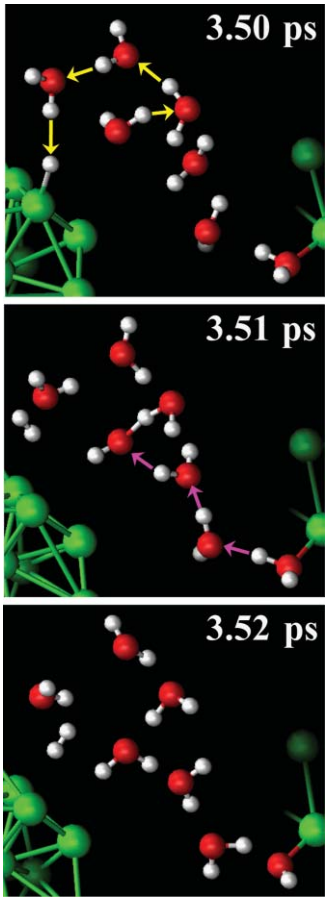

FIG. 7. Production process of the third hydrogen molecule on the Al cluster observed in MD simulation. Atomic configurations at time $t = 3.50$, 3.51, and 3.52 ps, where white, red, and green spheres represent H, O, and Al atoms, respectively. Yellow and magenta arrows represent the motion of H atoms.

3.52 ps). We should note that this process is influenced by the periodic boundary condition (see the periodic image of the Al cluster at the right edge of each snapshot in Fig. 7). Nevertheless, a similar reaction is expected to occur, if two Al clusters approach to each other in water. Even with one Al cluster, the Grotthuss mechanism still allows such a reaction to occur between Lewis-base and Lewis-acid sites, which are relatively far apart from each other on the cluster surface.

In all processes shown in Figs. 3–7, a hydrogen atom is generated before the formation of the H_2 molecule. Figure 8 shows atomic configurations for the adsorption of a hydrogen atom on the Al cluster during the MD simulation, which shows how the Grotthuss mechanism assists the production of hydrogen molecules. Two of the total of three hydrogen atoms on the surface of the Al cluster in Figs. 4 and 7 are generated in this way. The reaction begins with the dissociation of a H_2O molecule bonding to an Al atom (the magenta circle in Fig. 8), as one of its hydrogen atoms moves toward a neighboring H_2O molecule to form a hydronium ion (H_3O^+). This is followed by a chain of hydrogen bond switching events (denoted by the yellow arrows in Fig. 8) that involves in total of four H_2O molecules, and finally a hydrogen atom bonds to an Al atom after 190 fs (the cyan circle in Fig. 8). This process

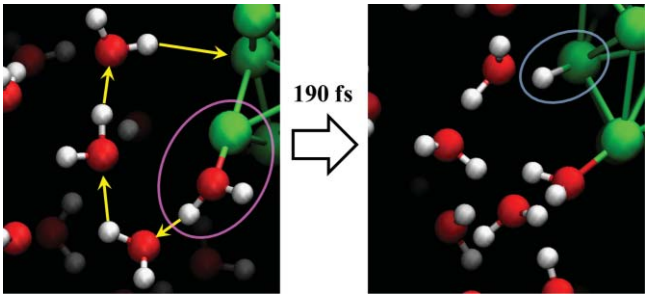

FIG. 8. Adsorption of a hydrogen atom on the Al cluster through the Grotthuss mechanism observed in MD simulation.

is summarized as

$$\mathrm{Al{-}OH_2} + 3\mathrm{H_2O} + \mathrm{Al'} \rightarrow \mathrm{Al{-}OH} + 3\mathrm{H_2O} + \mathrm{Al'{-}H}, \tag{2}$$

where Al and Al′, respectively, denote the aluminum atoms with Lewis acid and base characters involved in the reaction. This proton transfer is induced by the Lewis acid-base characters of the participating Al atoms.[17] (Similar phenomena were observed in water with hydrogen-bonded acid-base complexes[43] or charged solutes.[44])

Another process of hydrogen-atom adsorption on the Al cluster observed in MD simulation is shown in Fig. 9. As displayed in the snapshot at 1.97 ps (Fig. 9(b)), a water molecule, consisting of O3, H5, and H8, approaches to an Al atom labeled Al6. The chemical bond is formed between O3 and Al6, as $O_{ij}(t)$ for these atoms begins to increase around 1.97 ps (Fig. 9(a)). One of the OH bonds within the water molecule is broken, and hydrogen atom H5 is attached to the Al cluster as seen in the atomic configuration at 2.02 ps. $O_{\mathrm{O3–H5}}(t)$ decreases abruptly to zero at about 2 ps, while $O_{\mathrm{O3–H8}}(t)$ maintains finite values. This reaction is summarized as

$$\mathrm{Al{-}OH_2{+}Al'} \rightarrow \mathrm{Al{-}OH} + \mathrm{Al'{-}H}. \tag{3}$$

Note that this process is influenced by an extra water molecule. Since $O_{\mathrm{O3–H9}}(t)$ has small but finite values during the reaction, a weak covalentlike interaction exists between O3 and H9, which assists H5 in breaking the O3–H5 bond.

B. Activation energy

To find the minimum energy paths of chemical reactions, we adopt the nudged elastic band (NEB) method.[45,46] As a discrete representation of a path from the reactant configuration $\mathbf{R}_0$ to the product configuration $\mathbf{R}_M$, $M-1$ replicas of the system are created and connected together with springs. The images are then relaxed toward the minimum energy path. In this paper, we use $M = 15$–28.

The NEB method gives energy profiles at zero temperature. We also study the effect of finite temperatures on chemical reactions by calculating free energies. For this purpose, additional *ab initio* MD simulations are carried out at temperature $T = 300$ K by imposing geometrical constraints to obtain the free energy profile[47] along the reaction path. The Lagrange multiplier $\lambda(r)$ is introduced to constrain the distance r between atoms to be reacted. By taking time average,

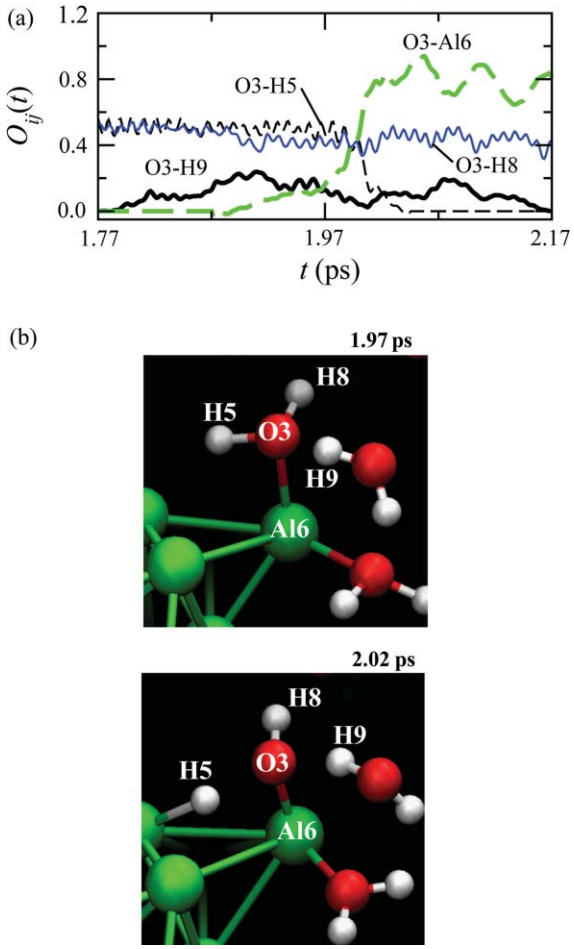

FIG. 9. Adsorption of a hydrogen atom on the Al cluster observed in MD simulation. (a) Time evolution of bond-overlap populations $O_{ij}(t)$ associated with atoms labeled in the snapshots of atomic configurations. (b) Atomic configurations at time $t = 1.97$ and 2.02 ps, where white, red, and green spheres represent H, O, and Al atoms, respectively.

we obtain the average Lagrange multiplier $\langle\lambda(r)\rangle$. The canonical-ensemble simulation at the room temperature is carried out for 1 ps at each distance r. The average Lagrange multiplier $\langle\lambda(r)\rangle$ becomes zero at an equilibrium distance r_0. The value of r is decreased (or increased depending on the reaction path) from this distance, and again $\langle\lambda(r)\rangle$ becomes zero at a critical distance r_d of the energy barrier. The relative free energies are obtained for $r_0 \geq r \geq r_\mathrm{d}$ by the following integral:[48]

$$\Delta F(r) = \int_{r_0}^{r} \langle\lambda(r')\rangle \mathrm{d}r'. \tag{4}$$

In order to estimate the rate of the hydrogen-production reaction, Eq. (1), we calculate the energy profile along the corresponding reaction path, using a system consisting of an isolated Al cluster, one H_2O molecule, and one extra H atom. In the initial configuration, a H_2O molecule is placed on the Lewis acid site on the Al cluster,[17] and the extra H atom is introduced on one of the Lewis base sites. From the result shown by the dashed line in Fig. 10, the activation energy is estimated by the NEB method to be $\Delta = 0.1$ eV. The finite-temperature effect by calculating the activation free energy

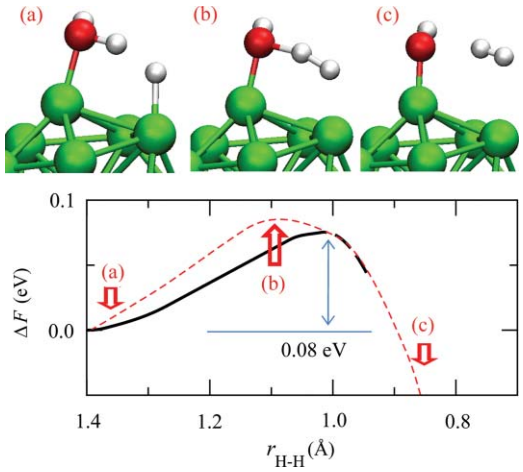

FIG. 10. (Lower panel) Free-energy profile (solid curve) at a temperature of 300 K along the reaction path of molecular hydrogen production, Al–OH_2 + Al–H → Al–OH + Al + H_2, as a function of the distance $r_{H–H}$ between the two hydrogen atoms that form a hydrogen molecule. The dashed curve is the energy profile obtained by NEB calculation. (Upper panel) Atomic configurations by NEB with $r_{H–H}$ = (a) 1.35, (b) 1.30, and (c) 0.85 Å.

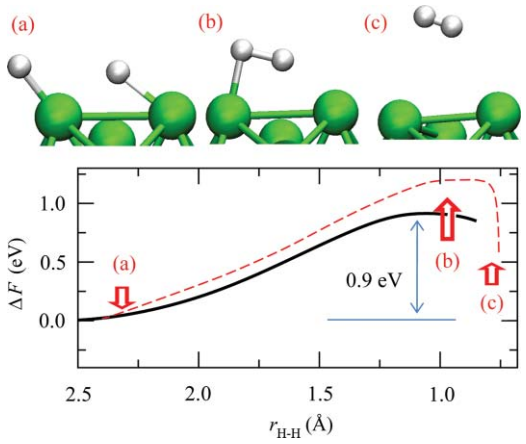

FIG. 12. (Lower panel) Free-energy profile (solid curve) at a temperature of 300 K along the reaction path of molecular-hydrogen production, Al–H + Al–H → Al + Al + H_2, as a function of the distance $r_{H–H}$ between the two hydrogen atoms that form a hydrogen molecule. The dashed curve is the energy profile obtained by NEB calculation. (Upper panel) Atomic configurations by NEB with $r_{H–H}$ = (a) 2.30, (b) 0.95, and (c) 0.80 Å.

gives a nearly identical value, $\Delta = 0.08$ eV, at 300 K (see the solid line in Fig. 10). The corresponding reaction rate is estimated as $k_{H_2} = (k_B T/h)\exp(-\Delta/k_B T) = 10^{11}$ (s^{-1}) at room temperature ($T = 300$ K) according to the transition state theory,[49] where k_B is the Boltzmann constant and h is the Planck constant.

We also examine several other reactions of the Al cluster with water to see whether they are competitive with the mechanism shown in Fig. 10. One possible product of Al-water reaction is Al–O, the production rate of which may be estimated as follows. To oxidize an Al cluster, the hydroxide ions on the Al cluster must dissociate as, e.g., Al–OH + Al–H → Al–O + Al + H_2. It is found that the activation free energy for this reaction is about 0.7 eV (Fig. 11), which is nine times larger than that for the Al–OH formation.

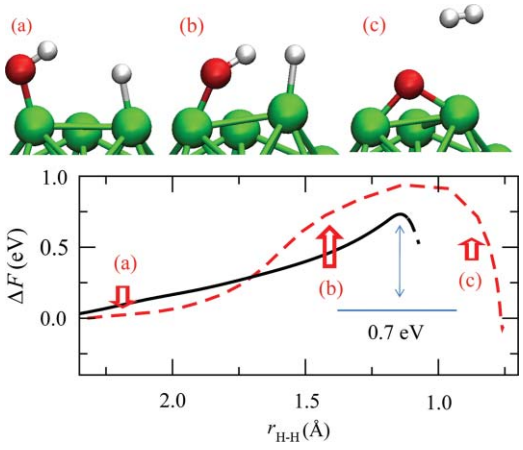

FIG. 11. (Lower panel) Free-energy profile (solid curve) at a temperature of 300 K along the reaction path of molecular-hydrogen production, Al–OH + Al–H → Al–O + Al + H_2 as a function of the distance $r_{H–H}$ between the two hydrogen atoms that form a hydrogen molecule. The dashed curve is the energy profile obtained by NEB calculation. (Upper panel) Atomic configurations by NEB with $r_{H–H}$ = (a) 2.20, (b) 1.40, and (c) 0.85 Å.

Another possible reaction is the formation of a hydrogen molecule from two hydrogen atoms on an Al cluster, Al–H + Al–H → Al + Al + H_2, with an activation free energy of 0.9 eV (Fig. 12). This is the same mechanism proposed for H_2 production in gas phase,[17] for which the activation barrier is an order-of-magnitude higher than that for Al–OH_2 + Al–H → Al–OH + Al + H_2.[50]

As was shown in Fig. 8, a hydrogen atom is generated on the Al cluster by the Grotthuss mechanism prior to the production of a hydrogen molecule. To estimate the energy barrier for this process, we calculate the energy profile by the NEB method along the reaction path for the production of a hydroxide group and a hydrogen atom on the Al cluster:

$$\mathrm{Al{-}OH_2} + m\mathrm{H_2O} + \mathrm{Al'} \rightarrow \mathrm{Al{-}OH} + m\mathrm{H_2O} + \mathrm{Al'{-}H}, \tag{5}$$

where $m = 3$ for the process observed in the MD simulation shown in Fig. 8. In Eq. (5), Al and Al′ denote the aluminum atoms with Lewis acid and base characters, respectively, involved in the reaction. Figure 13 shows the activation barriers for different values of m. The energy barrier has the highest value, $\Delta = 0.42$ eV, when only a single H_2O molecule ($m = 0$) is involved (open circles). This energy barrier is lowered when extra bulk H_2O molecules are incorporated, i.e., $m \geq 1$. The lowest energy barrier is $\Delta = 0.20$ eV for the case of $m = 1$ (solid circles). The energy barriers for $m = 2$ and 3 are $\Delta = 0.25$ and 0.30 eV, respectively. Note that the energy barrier increases at a rate of about 0.05 eV/molecule for $m > 1$. From these values, the energy barrier for Eq. (5) is estimated to be $\Delta = 0.15 + 0.05m$ eV for $m \geq 1$, which indicates that the energy to split H_2O into H^+ and OH^- is 0.15 eV and the energy to form one hydronium ion (H_3O^+) is 0.05 eV in the reaction with extra bulk H_2O as well as one H_2O bonded to the Al cluster. The rates of these reactions at room temperature are estimated to be $k_1 = (k_B T/h)\exp(-\Delta/k_B T) \approx 10^7 - 10^9$ s^{-1}.

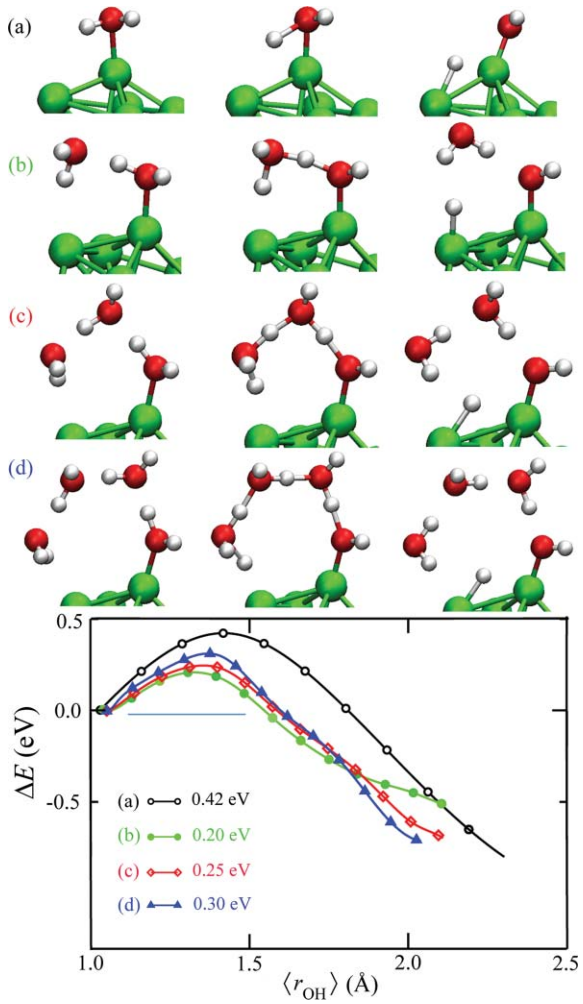

FIG. 13. (Lower panel) Energy profiles along the reaction paths for the production of a hydroxide ion and a hydrogen atom on an Al cluster through the Grotthuss mechanism, Al–OH_2 + mH_2O + Al′ → Al–OH + mH_2O + Al′–H with (a) $m = 0$ (black open circles), (b) $m = 1$ (green solid circles), (c) $m = 2$ (red open diamonds), and (d) $m = 3$ (blue solid triangle), obtained by NEB calculations. $\langle r_{OH} \rangle$; is the average length of OH bonds that are broken in the reaction. (Upper panel) Initial, middle, and final atomic configurations by NEB for the paths (a), (b), (c), and (d).

In the process shown in Fig. 8, the Al–OH product of Eq. (2) is quickly converted back to Al–H_2O again by the Grotthuss mechanism, which involves a third Al atom (denoted as Al″) with an adsorbed water molecule:

$$\mathrm{Al{-}OH} + m\mathrm{H_2O} + \mathrm{Al''} - \mathrm{OH_2} \rightarrow \mathrm{Al{-}OH_2} + m\mathrm{H_2O} + \mathrm{Al''} - \mathrm{OH}. \quad (6)$$

Figure 14 shows the energy profiles for the reaction of Eq. (6) for different values of m. The activation energy of this reaction is estimated to be 0.10, 0.03, and 0.04 eV for $m = 1$, 2, and 3, respectively. The corresponding rate is $k_2 = 10^{11} - 10^{12}\ \mathrm{s}^{-1} \gg k_1$ at 300 K. The combined reactions, Eqs. (5) and (6), have the rate of $k_H = \min(k_1, k_2) = 10^7 - 10^9\ \mathrm{s}^{-1}$, and their end products, Al–OH_2 + Al″–H, become the reactants of the hydrogen-production reaction, Eq. (1).

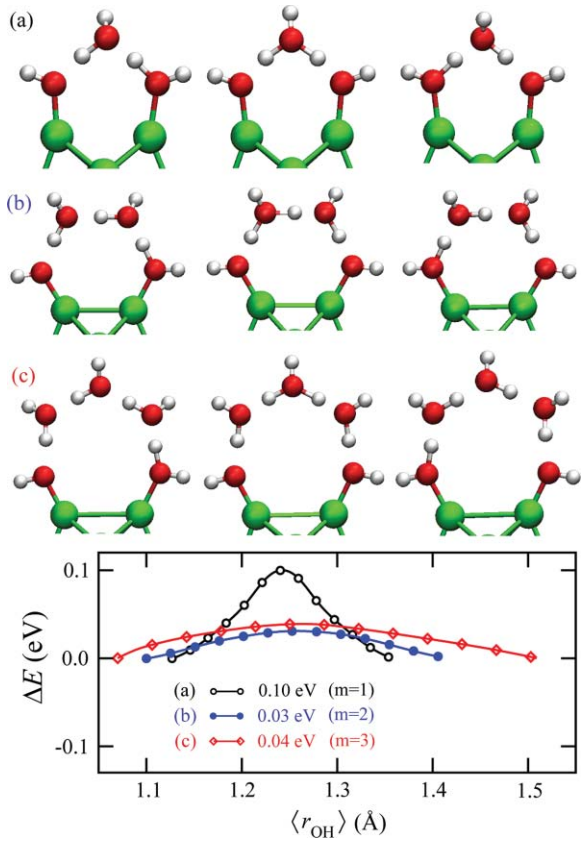

FIG. 14. (Lower panel) Energy profiles along the reaction Al–OH + mH_2O + Al″–OH_2 → Al–OH_2 + mH_2O + Al″–OH with (a) $m = 1$ (black open circles), (b) $m = 2$ (blue solid circles), and (c) $m = 3$ (red open diamonds), obtained by NEB calculations. $\langle r_{OH} \rangle$; is the average length of OH bonds that are broken in the reaction. (Upper panel) Initial, middle, and final atomic configurations by NEB for the paths (a), (b), and (c).

The reactions found in our simulations are very rapid with the rate-limiting step of $k_H = 10^7 - 10^9\ (\mathrm{s}^{-1})$ at 300 K. The reaction specificity and efficiency achieved by superatoms and autocatalytic behavior of water presented here may be applicable to much broader applications, e.g., direct splitting of water using photocatalysts.[51–53]

IV. SUMMARY

The overall mechanism of H_2 production by the Al cluster in water is summarized as follows. First, an oxygen atom in a water molecule bonds to an Al atom with the Lewis-acidic character. This enhances the Lewis-basic character of surrounding Al atoms, and, in turn, a hydrogen atom is generated at a surrounding Lewis-base site assisted by rapid proton transport. Although it is hard for the water molecule to dissociate by itself, the Grotthuss mechanism greatly reduces the activation barrier for the dissociation. Finally, a hydrogen molecule is produced from the water molecule and the hydrogen atom on the Al cluster, which has a lower activation barrier than that for hydrogen-atom generation. Since the resulting hydroxide ion has a strong Lewis-base character and returns to a water molecule again through the Grotthuss mechanism, each Lewis acid-base pair can produce multiple hydrogen molecules in acidic conditions.

ACKNOWLEDGMENTS

This work was supported by U.S. Department of Energy, Office of Basic Energy Sciences, Materials Sciences & Engineering Division, Theoretical Condensed Matter Physics Program, Grant No. DE-FG02-04ER46130 and a Grant-in-Aid for JSPS Fellows. S.O. and F.S. acknowledge support by Hamamatsu Photonics K.K., Japan. Simulations were performed at the Research Computing Facility and the Collaboratory for Advanced Computing and Simulations of the University of Southern California.

[1] A. Steinfeld, Sol. Energy **78**, 603 (2005).
[2] T. Yabe, S. Uchida, K. Ikuta, K. Yoshida, C. Baasandash, M. S. Mohamed, Y. Sakurai, Y. Ogata, M. Tuji, Y. Mori, Y. Satoh, T. Ohkubo, M. Murahara, A. Ikesue, M. Nakatsuka, T. Saiki, S. Motokoshi, and C. Yamanaka, Appl. Phys. Lett. **89**, 261107 (2006).
[3] T. Kodama and N. Gokon, Chem. Rev. **107**, 4048 (2007).
[4] M. Roeb and H. Muller-Steinhagen, Science **329**, 773 (2010).
[5] J. Petrovic and G. Thomas, *Reaction of Aluminum with Water to Produce Hydrogen* (U.S. Department of Energy, Washington, DC, 2008).
[6] G. W. Crabtree and N. S. Lewis, Phys. Today **60**(3), 37 (2007).
[7] N. S. Lewis, Science **315**, 798 (2007).
[8] Y. Huang, G. A. Risha, V. Yang, and R. A. Yetter, Combust. Flame **156**, 5 (2009).
[9] Y. Q. Yang, S. F. Wang, Z. Y. Sun, and D. D. Dlott, Appl. Phys. Lett. **85**, 1493 (2004).
[10] B. J. Henz, T. Hawa, and M. R. Zachariah, J. Appl. Phys. **107**, 024901 (2010).
[11] V. I. Levitas, B. W. Asay, S. F. Son, and M. Pantoya, Appl. Phys. Lett. **89**, 071909 (2006).
[12] F. Shimojo, A. Nakano, R. K. Kalia, and P. Vashishta, Appl. Phys. Lett. **95**, 043114 (2009).
[13] S. K. R. S. Sankaranarayanan, E. Kaxiras, and S. Ramanathan, Phys. Rev. Lett. **102**, 095504 (2009).
[14] M. Haruta, Nature (London) **437**, 1098 (2005).
[15] M. Valden, X. Lai, and D. W. Goodman, Science **281**, 1647 (1998).
[16] B. Yoon, H. Hakkinen, U. Landman, A. S. Worz, J. M. Antonietti, S. Abbet, K. Judai, and U. Heiz, Science **307**, 403 (2005).
[17] P. J. Roach, W. H. Woodward, A. W. Castleman, A. C. Reber, and S. N. Khanna, Science **323**, 492 (2009).
[18] A. C. Reber, S. N. Khanna, P. J. Roach, W. H. Woodward, and A. W. Castleman, J. Phys. Chem. A **114**, 6071 (2010).
[19] D. E. Bergeron, A. W. Castleman, T. Morisato, and S. N. Khanna, Science **304**, 84 (2004).
[20] C. J. Wu, L. E. Fried, L. H. Yang, N. Goldman, and S. Bastea, Nat. Chem. **1**, 57 (2009).
[21] E. Vöhringer-Martinez, B. Hansmann, H. Hernandez, J. S. Francisco, J. Troe, and B. Abel, Science **315**, 497 (2007).
[22] N. Agmon, Chem. Phys. Lett. **244**, 456 (1995).
[23] D. Marx, M. E. Tuckerman, J. Hutter, and M. Parrinello, Nature (London) **397**, 601 (1999).
[24] H. S. Kato, K. Akagi, S. Tsuneyuki, and M. Kawai, J. Phys. Chem. C **112**, 12879 (2008).
[25] F. Shimojo, S. Ohmura, R. K. Kalia, A. Nakano, and P. Vashishta, Phys. Rev. Lett. **104**, 126102 (2010).
[26] P. E. Blöchl, Phys. Rev. B **50**, 17953 (1994).
[27] G. Kresse and D. Joubert, Phys. Rev. B **59**, 1758 (1999).
[28] J. P. Perdew, K. Burke, and M. Ernzerhof, Phys. Rev. Lett. **77**, 3865 (1996).
[29] S. G. Louie, S. Froyen, and M. L. Cohen, Phys. Rev. B **26**, 1738 (1982).
[30] J. Ihm, A. Zunger, and M. L. Cohen, J. Phys. C: Solid State Phys. **12**, 4409 (1979).
[31] G. Kresse and J. Hafner, Phys. Rev. B **49**, 14251 (1994).
[32] F. Shimojo, R. K. Kalia, A. Nakano, and P. Vashishta, Comput. Phys. Commun. **140**, 303 (2001).
[33] S. Nosè, Mol. Phys. **52**, 255 (1984).
[34] W. G. Hoover, Phys. Rev. A **31**, 1695 (1985).
[35] M. Tuckerman, B. J. Berne, and G. J. Martyna, J. Chem. Phys. **97**, 1990 (1992).
[36] R. S. Mulliken, J. Chem. Phys. **23**, 1833 (1955).
[37] R. S. Mulliken, J. Chem. Phys. **23**, 1841 (1955).
[38] D. Sánchez-Portal, E. Artacho, and J. M. Soler, J. Phys. Condens. Matter **8**, 3859 (1996).
[39] M. D. Segall, R. Shah, C. J. Pickard, and M. C. Payne, Phys. Rev. B **54**, 16317 (1996).
[40] F. Shimojo, A. Nakano, R. K. Kalia, and P. Vashishta, Phys. Rev. E **77**, 066103 (2008).
[41] O. F. Sankey and D. J. Niklewski, Phys. Rev. B **40**, 3979 (1989).
[42] J. M. Soler, E. Artacho, J. D. Gale, A. García, J. Junquera, P. Ordejón, and D. Sánchez-Portal, J. Phys. Condens. Matter **14**, 2745 (2002).
[43] M. Rini, B. Z. Magnes, E. Pines, and E. T. J. Nibbering, Science **301**, 349 (2003).
[44] P. L. Geissler, C. Dellago, D. Chandler, J. Hutter, and M. Parrinello, Science **291**, 2121 (2001).
[45] H. Jonsson, G. Mills, and K. Jacobsen, *Classical and Quantum Mechanics in Condensed Phase Simulations* (World Scientific, Singapore, 1998).
[46] G. Henkelman and H. Jonsson, J. Chem. Phys. **113**, 9978 (2000).
[47] K. C. Hass, W. F. Schneider, A. Curioni, and W. Andreoni, Science **282**, 265 (1998).
[48] A. Curioni, M. Sprik, W. Andreoni, H. Schiffer, J. Hutter, and M. Parrinello, J. Am. Chem. Soc. **119**, 7218 (1997).
[49] D. G. Truhlar, B. C. Garrett, and S. J. Klippenstein, J. Phys. Chem. **100**, 12771 (1996).
[50] We have not observed any dissociation of the hydroxide ions (Al–OH) and any molecular-hydrogen formation from two H atoms on the Al cluster in our MD simulation, which is consistent with its estimated high activation barriers.
[51] Z. G. Zou, J. H. Ye, K. Sayama, and H. Arakawa, Nature (London) **414**, 625 (2001).
[52] K. Maeda, K. Teramura, D. L. Lu, T. Takata, N. Saito, Y. Inoue, and K. Domen, Nature (London) **440**, 295 (2006).
[53] M. W. Kanan and D. G. Nocera, Science **321**, 1072 (2008).